Current-Induced Spin Polarization in Anisotropic Spin-Orbit Fields

B. M. Norman,[1] C. J. Trowbridge,[1] D. D. Awschalom,[2] and V. Sih[1],[*]

[1]*Department of Physics, University of Michigan, Ann Arbor, Michigan 48109, USA*
[2]*Institute for Molecular Engineering, University of Chicago, Chicago, Illinois 60637, USA*

The magnitude and direction of current-induced spin polarization and spin-orbit splitting are measured in $In_{0.04}Ga_{0.96}$ As epilayers as a function of in-plane electric and magnetic fields. We show that, contrary to expectation, the magnitude of the current-induced spin polarization is smaller for crystal directions corresponding to larger spin-orbit fields. Furthermore, we find that the steady-state in-plane spin polarization does not align along the spin-orbit field, an effect due to anisotropy in the spin relaxation rate.

Current-induced spin polarization (CISP) is a phenomenon in which carrier spins are oriented when subjected to current flow. As an all-electrical method of generating spin polarization in nonmagnetic materials, it may be useful for applications such as spin-based information processing [1] and the electrical control of magnetization [2]. Existing theory predicts that the spin polarization should be proportional to the spin-orbit (SO) splitting, yet no clear trend has been observed. Thus, the mechanism that produces this spin polarization remains an open question.

Electrical spin orientation was first proposed by Ivchenko and Pikus [3], and its inverse effect, photocurrent induced by absorption of circularly polarized light, was observed by Vorob'ev *et al.* in tellurium [4]. It was proposed [5] and subsequently measured in strained III–V epilayers [6] and in quantum wells and two-dimensional electron gases [7–9]. Electrically generated spin polarization has also been observed in GaN crystals having a weak spin-orbit interaction [10] and in ZnSe having no measurable SO splitting [11]. Time-resolved measurements indicate that electron spins orient along the spin-orbit field within picoseconds and then precess about the sum of the external and SO fields [6,12].

Aronov, Lyanda-Geller, and Pikus [13] attributed a polarization of spins by current to two dominant mechanisms: the equilibrium orientation of spins along the spin-orbit effective magnetic field and a nonequilibrium state filling for electrons that undergo scattering accompanied by a spin flip. Engel, Rashba, and Halperin explained the observed out-of-plane spin polarization by using a model that requires anisotropic scattering and nonparabolic bands [14]. In these studies, it was predicted that the current-induced spin polarization magnitude is proportional to the spin-orbit splitting.

In this Letter, we investigate the effect of a momentum **k**-dependent spin-orbit interaction on the magnitude of current-induced spin polarization. Samples are patterned to allow arbitrary orientation of the electron drift momentum and an external magnetic field in the epilayer plane.

By varying the drift momentum direction, we also vary the strength and orientation of the anisotropic spin-orbit effective magnetic field. In this way, we can tune the strength of the spin-orbit splitting while holding other material parameters constant. We find that, for a given momentum direction, both the current-induced spin polarization and spin-orbit field magnitudes are proportional to the electron drift velocity. However, the ratio of the CISP and SO field coefficients obeys a negative differential relationship. For electron momentum along the crystal direction having the strongest SO field, the CISP magnitude is weakest. Furthermore, the same SO splitting in two samples with different SO field anisotropies corresponds to different CISP magnitudes. Finally, we show that the steady-state in-plane spin polarization does not align along the spin orientation direction, even in the absence of precession. We present a model requiring anisotropic spin relaxation that explains this effect.

Five samples in this study are processed from the same wafer of 500 nm $In_{0.04}Ga_{0.96}$ As grown on undoped (001) GaAs by using molecular beam epitaxy. The InGaAs epilayer is Si-doped at 3×10^{16} cm^{-3}. Samples *A* and *B* are etched in a cross pattern [Fig. 1(a)], while samples *C–E* have defined channels along [110] and [1$\bar{1}$0]. The cross pattern is used to provide current along any arbitrary direction in the (001) plane [15]. The electric field is calculated by using relaxation methods.

The spin-orbit effective magnetic field arises from inversion asymmetry and strain-induced band splitting [16,17]. Bulk inversion asymmetry (BIA) and structural inversion asymmetry (SIA) give rise to the Dresselhaus [18] and Rashba [19] spin-orbit fields, respectively. Biaxial strain due to lattice mismatched growth has the same directional dependence as the linear Dresselhaus field, and the two can be combined into a single BIA-like field. Furthermore, uniaxial strain along [110] due to strain relaxation has the same directional dependence as the Rashba field, and the two can be combined into a single SIA-like field. The SO Hamiltonians can be described by
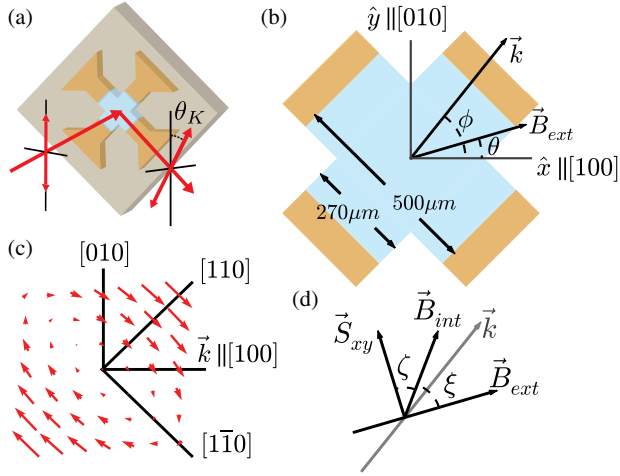
(a)

(b)

(c)

(d)

FIG. 1 (color online).   (a) InGaAs epilayer (blue) is etched into cross patterns with four electrical contacts (orange) on the GaAs substrate (gray). Kerr rotation measures the component of spin polarization along the laser axis ($\hat{z}$). (b) Voltages applied to the contacts determine the electron drift momentum $\vec{k}$, at angle ϕ with respect to the [100] crystal direction. $\vec{B}_{ext}$ is oriented at angle θ by rotating the cryostat. (c) Total SO field as a function of $\vec{k}$ from SIA and BIA components with relative strength $\alpha/\beta = 2$ and $\alpha > 0$. (d) The SO field $\vec{B}_{int}$ makes an angle ξ with respect to the external magnetic field $\vec{B}_{ext}$. The steady-state in-plane spin polarization $\vec{S}_{xy}$ is shifted from $\vec{B}_{int}$ by angle ζ. The measured CISP is maximized when $\zeta + \xi = 90°$. We take $\vec{\gamma} \parallel \vec{B}_{int}$.

$$H_{SO} = (\alpha k_y + \beta k_x)\sigma_x - (\alpha k_x + \beta k_y)\sigma_y, \quad (1)$$

where α represents the strength of the SIA-like field and β represents the strength of the BIA-like field. It is observed that $\beta > 0$ due to the known sign of the biaxial strain coefficient. On the other hand, the uniaxial strain component is inhomogeneous, and the sign of α changes across the different samples studied from the wafer. We exploit this inhomogeneity to obtain samples from the same wafer that have different ratios of α/β. Figure 1(c) displays the total SO field for $\alpha/\beta = 2$. The extremum SO fields occur for **k** along [110] and [1$\bar{1}$0]. The four-contact pattern allows for continuous tuning between these extremes.

The experimental geometry is shown in Fig. 1(b). An external electromagnet provides an applied magnetic field. Samples are mounted in a liquid helium flow cryostat on a rotation stage that allows for orientation of the magnetic field to an angle θ with respect to the [100] crystal axis ($\hat{x}$). The voltages applied to the four contacts determine the magnitude and orientation (ϕ) of the electric field. In this way, current-induced spin polarization and the spin-orbit fields can be measured while the external electric and magnetic field directions are independently varied along any direction in the (001) plane.

Measurements of the spin-orbit field are conducted by using a pump-probe procedure [17]. A mode-locked Ti:

sapphire laser tuned to the band edge ($\lambda = 845$ nm) is split into pump and probe pulses. The circularly polarized pump excites spin-polarized carriers into the conduction band according to the optical selection rules [20]. A two-axis steering mirror in the pump path allows for spatial positioning of the pump-induced spin packet. A time-delayed ($\Delta t = 13$ ns) and spatially separated linearly polarized probe pulse undergoes optical Kerr rotation (KR) [Fig. 1(a)], the angle of which is proportional to the $\hat{z}$ component of the spin polarization [21] which will be presented throughout in units of μrad. We estimate that a Kerr rotation angle of $1\,\mu$rad corresponds to a degree of polarization of $\sim 1 \times 10^{-4}$ [6]. The KR of the probe pulse is described by

$$\theta_K = \theta_{op} \cos\left(\frac{g\mu_B \Delta t}{\hbar}\sqrt{(B_{ext} + B_{\parallel})^2 + B_{\perp}^2}\right), \quad (2)$$

where μ_B is the Bohr magneton, $\hbar$ is the reduced Planck's constant, g is the electron g factor, θ_{op} is the KR amplitude, and $B_{\perp}$ and $B_{\parallel}$ are the components of the SO field perpendicular and parallel to **B**$_{ext}$, respectively.

Figure 2(a) shows a set of spin-orbit field measurements for $\theta = \phi = 15°$ at several voltages. For samples A and B, ϕ is varied from $-45°$ to $+45°$. We orient **k** ∥ **B**$_{ext}$ to extract the components of **B**$_{int}$ parallel and perpendicular to **k**. The drift velocity (v_d) of the spin packet is determined for each applied voltage from the pump-probe spatial separation (x_c) at the maximum overlap amplitude [Fig. 2(b)]. The SO field components as a function of v_d [Fig. 2(e)] are extracted from the magnitude of $B_{\perp}$ [Fig. 2(c)] and $B_{\parallel}$ [Fig. 2(d)] evaluated at x_c. We find that the SO field is proportional to the electron drift velocity and use this proportionality constant (κ) to characterize the strength of the SO field. The magnitude and direction of the spin-orbit field are plotted in Figs. 2(f) and 2(g), respectively. Lines are fits to the total SO field described by Eq. (1). The deviation from the expected curve may be due to an additional strain axis arising from strain relaxation as the epilayer is grown beyond the critical thickness. This underscores the importance of directly measuring the spin-orbit field for each momentum direction for comparison with the magnitude of current-induced spin polarization.

We describe current-induced spin polarization phenomenologically by assuming a spin-dependent relaxation rate:

$$\Gamma_{\downarrow(\uparrow)} = \Gamma + (-)\gamma, \quad (3)$$

where Γ is the average spin relaxation rate and γ represents the difference in scattering rates between up and down spins. By using the semiclassical Boltzmann transport equation [13] assuming a steady-state conduction band population, the time dependence of the spin polarization is described as follows:

$$\frac{\partial \vec{S}}{\partial t} = -\overleftrightarrow{\Gamma} \cdot \vec{S} + \vec{\Omega} \times \vec{S} + \vec{\gamma}, \quad (4)$$
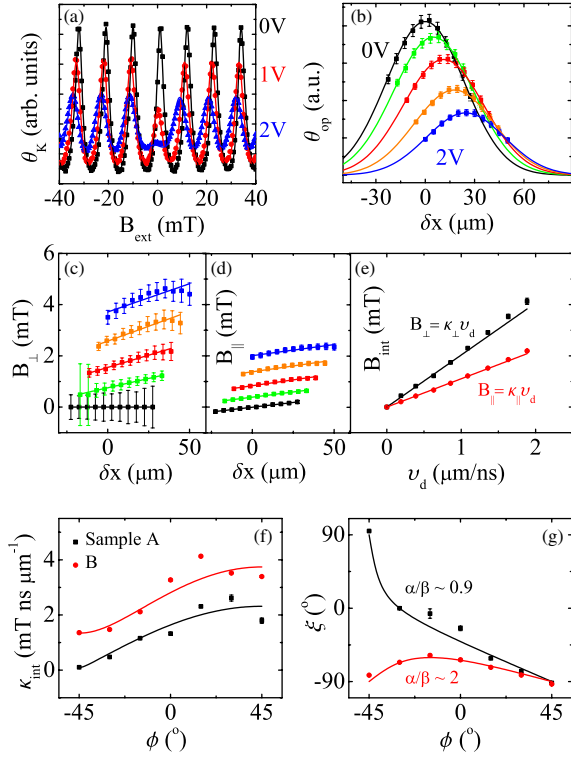
FIG. 2 (color online).   (a) Kerr rotation as a function of $\mathbf{B}_{ext}$ at a fixed pump-probe time delay for external voltages of 0 (black squares), 1 (red circles), and 2V (blue triangles) fit to Eq. (2). (b) The location of the spin packet center from the fit amplitude (θ_{op}) gives the electron drift velocity as a function of voltage. (c),(d) Components of the SO field perpendicular and parallel to $\mathbf{B}_{ext}$ as a function of pump-probe separation. (e) The slope (κ) of $\mathbf{B}_{int}$ evaluated at the spin packet center is used to characterize the strength of the SO field. (f),(g) The SO field coefficient (κ) and direction (ξ) are measured as a function of the electron momentum direction (ϕ) for samples A (black squares) and B (red circles). In (a)–(e), the data set is taken from sample A for $\theta = \phi = 15°$. Voltage measurements are taken at linear spacings between 0 (black) and 2 V (blue).

where $\vec{S}$ represents the vector spin polarization, $\vec{\Omega}$ the Larmor precession frequency given by $\vec{\Omega} = (g\mu_B/\hbar)$ $(\vec{B}_{ext} + \vec{B}_{int})$, and $\vec{\gamma}$ the vector spin polarization generated per unit time as a result of CISP. $\vec{\gamma}$ is expected to be independent of $\vec{S}$ for small polarizations [6], and we take it to align along $\mathbf{B}_{int}$ such that $\vec{\gamma} = \gamma[\cos(\xi)\hat{x}' + \sin(\xi)\hat{y}']$ (i.e., $\gamma_z = 0$), with the definition of a new primed basis with $\hat{x}' \| \mathbf{B}_{ext}$ and $\hat{z}' = \hat{z}$.

The spin dephasing rate tensor is, in general, anisotropic and obtained from the D'yakonov-Perel dephasing mechanism [20]. It is described in the $[1\bar{1}0]$, $[110]$, and $[001]$ eigenbases by

$$\overleftrightarrow{\Gamma} = \frac{1}{\tau_0(v_d)} \begin{pmatrix} (1+r)^2 & 0 & 0 \\ 0 & (1-r)^2 & 0 \\ 0 & 0 & 2(1+r^2) \end{pmatrix}, \quad (5)$$
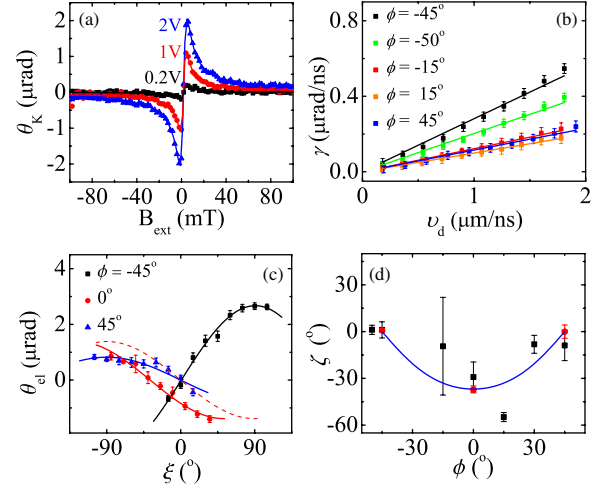

FIG. 3 (color online).   (a) CISP measurements at 0.2 (black squares), 1 (red circles), and 2 V (blue triangles). The lines are fits to Eq. (7). (b) The magnitude of the spin orientation per unit time γ as a function of drift velocity for several $\mathbf{k}$ directions. The slope η is used to characterize the CISP magnitude. (c) CISP amplitude as a function of angle (ξ) between $\mathbf{B}_{ext}$ and $\mathbf{B}_{int}$ for $\phi = -45°$ (black squares), $0°$ (red circles), and $+45°$ (blue triangles) all taken at an applied voltage of 2 V. Solid lines are fits to a sine curve. θ_{el} is maximized when $\vec{S}_{xy} \perp \mathbf{B}_{ext}$. The dashed red line is the expected curve for $\phi = 0°$ if $\vec{S}_{xy} \| \vec{r}$; it is shifted from the experimental curve by $\sim 37°$. (d) Deviation (ζ) of in-plane spin polarization ($\vec{S}_{xy}$) from the CISP alignment vector ($\vec{\gamma}$) extracted from measurements in (c) (red circles) and from fits to Eq. (7) (black squares). The blue line is a curve expected from our model given by Eq. (6).

where $\tau_0(v_d)$ is the relaxation time in the absence of uniaxial strain. If the SO field is well described by Eq. (1) and the D'yakonov-Perel is the only dephasing mechanism present, we expect $r = \alpha/\beta$. Solving Eq. (4) in the absence of precession [22], we find that the steady-state in-plane spin polarization ($\vec{S}_{xy}$) is shifted from $\vec{\gamma}$ by an angle ζ given by

$$\zeta = \tan^{-1}\left[\frac{2r(\cos^2\phi - \sin^2\phi)}{1 - r^2}\right]. \quad (6)$$

We approximate the $\hat{z}$ component of the spin polarization by taking spins to align at a rate $\gamma = |\vec{\gamma}|$ along $\vec{S}_{xy}$ with an effective dephasing time τ (such that $|\vec{S}_{xy}| = \gamma\tau$) and precessing about the vector magnetic field. The measured spin polarization in this case is described by [22]

$$S_z = \theta_{el} \frac{\Omega_{ext}\tau + \Omega_{int}\tau \frac{\sin(\zeta)}{\sin(\zeta+\xi)}}{1 + (\Omega_{tot}\tau)^2}, \quad (7)$$

where $\theta_{el} = S_{xy}\sin(\zeta + \xi)$ is the measured electrically generated spin polarization and $\Omega_{tot}^2 = \Omega_{ext}^2 + \Omega_{int}^2 + 2\Omega_{ext}\Omega_{int}\cos(\xi)$.

Kerr rotation of a linearly polarized probe beam tuned to the low-energy side of the band edge ($\lambda = 851$ nm) in the
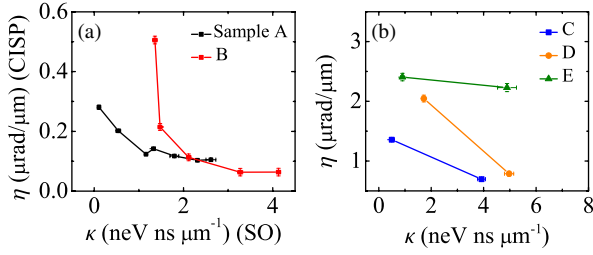
FIG. 4 (color online).   (a) CISP for various SO field magnitudes for different directions of **k** in samples *A* and *B*. A negative differential relationship is observed. (b) The same negative differential relationship is observed in samples *C*–*E* which have two channels patterned along [110] and [1$\bar{1}$0].

absence of optical pumping is used to measure the $\hat{z}$ component of the electrically induced spin polarization [6]. The relative strength of two phase-matched square wave sources across opposite contacts determines the angle ϕ of **k** with respect to [100]. For each choice of ϕ, we rotate the cryostat to scan the external magnetic field direction $\theta = \theta'$ such that the measured current-induced spin polarization is maximized (i.e., when $\vec{S}_{xy} \perp \mathbf{B}_{ext}$). An odd-Lorentzian line shape is observed [Fig. 3(a)] which is antisymmetric if $\vec{S}_{xy} \| \vec{\gamma} \perp \mathbf{B}_{ext}$ [12,22]. The amplitude and width give the electrically generated spin polarization amplitude (θ_{el}) and the effective dephasing time (τ), respectively. From these we can extract the spin generation per unit time γ. Figure 3(b) shows γ as a function of drift velocity for several orientations of **k**. It obeys a linear relationship and is fit to the equation $\gamma = \eta v_d$, where η is used to characterize the current-induced spin polarization magnitude.

By rotating the cryostat, we vary the angle (ξ) that $\vec{\gamma}$ makes with $\mathbf{B}_{ext}$. We measure θ_{el} as a function of this angle for **k** along [1$\bar{1}$0], [100], and [110] [Fig. 3(c)]. For **k** along [110] and [1$\bar{1}$0], θ_{el} is largest when $\vec{\gamma} \perp \mathbf{B}_{ext}$, indicating that the in-plane spin polarization ($\vec{S}_{xy}$) is along $\vec{\gamma}$, as expected. However, for **k** along [100], $\vec{\gamma}$ is no longer along an eigenstate of the relaxation tensor, and the in-plane spin polarization is shifted from $\vec{\gamma}$ by $\zeta \sim 37°$. We expect from Eq. (6) that ζ is maximized when **k** is along [100]. Figure 3(d) displays ζ extracted from the measurements in Fig. 3(c) (red circles) and as determined from fits to Eq. (7) (black squares) at an applied voltage of 2 V. The behavior of ζ as a function of ϕ expected from our model is described by Eq. (6) (blue line). We can see that the model and experimental data are consistent with each other.

Figure 4(a) shows the current-induced spin polarization coefficient η compared to the measured spin-orbit field coefficient κ for samples *A* and *B*. We see that CISP obeys a negative differential relationship with the SO field; for **k** aligned along the crystal direction having the weakest SO field, the CISP magnitude is strongest and vice versa. Furthermore, for each sample, there is a different ratio α/β due to inhomogeneous strain in the wafer corresponding to a different curve on which the data points lie. That is, CISP

appears to depend strongly on the anisotropy of the SO field for a given sample, rather than just on the magnitude of the SO field itself. The nature of this observed relationship is not well understood. To further corroborate this effect, Fig. 4(b) shows data from three samples (*C*–*E*) with two orthogonal channels oriented along [110] and [1$\bar{1}$0] which also show that the larger CISP coefficient occurs in the direction with the smaller SO coefficient.

In summary, we observe that the momentum directions that have the largest current-induced spin polarization also have the weakest spin-orbit field. It is clear from this relationship that CISP cannot depend on the SO splitting alone, but that some other effects must contribute, such as scattering accompanied by a spin flip [5] or amplification due to spin-dependent mobility [23]. Furthermore, the steady-state in-plane current-induced spin polarization $\vec{S}_{xy}$ only aligns along the internal field for directions that correspond to an eigenbasis state of the spin relaxation rate tensor.

*vsih@umich.edu
[1] D. D. Awschalom and M. E. Flatté, Nat. Phys. **3**, 153 (2007).
[2] A. Chernyshov, M. Overby, X. Liu, J. K. Furdyna, Y. Lyanda-Geller, and L. P. Rokhinson, Nat. Phys. **5**, 656 (2009).
[3] E. L. Ivchenko and G. E. Pikus, JETP Lett. **27**, 604 (1978).
[4] L. E. Vorob'ev, E. L. Ivchenko, G. E. Pikus, I. I. Farbshtein, V. A. Shalygin, and A. V. Shturbin, JETP Lett. **29**, 441 (1979).
[5] A. G. Aronov and Y. B. Lyanda-Geller, JETP Lett. **50**, 431 (1989).
[6] Y. K. Kato, R. C. Myers, A. C. Gossard, and D. D. Awschalom, Phys. Rev. Lett. **93**, 176601 (2004).
[7] V. Sih, R. C. Myers, Y. K. Kato, W. H. Lau, A. C. Gossard, and D. D. Awschalom, Nat. Phys. **1**, 31 (2005).
[8] C. L. Yang, H. T. He, L. Ding, L. J. Cui, Y. P. Zeng, J. N. Wang, and W. K. Ge, Phys. Rev. Lett. **96**, 186605 (2006).
[9] H. J. Chang, T. W. Chen, J. W. Chen, W. C. Hong, W. C. Tsai, Y. F. Chen, and G. Y. Guo, Phys. Rev. Lett. **98**, 136403 (2007).
[10] W. F. Koehl, M. H. Wong, C. Poblenz, B. Swenson, U. K. Mishra, J. S. Speck, and D. D. Awschalom, Appl. Phys. Lett. **95**, 072110 (2009).

[11] N. P. Stern, S. Ghosh, G. Xiang, M. Zhu, N. Samarth, and D. D. Awschalom, Phys. Rev. Lett. **97**, 126603 (2006).

[12] S. Kuhlen, K. Schmalbuch, M. Hagedorn, P. Schlammes, M. Patt, M. Lepsa, G. Güntherodt, and B. Beschoten, Phys. Rev. Lett. **109**, 146603 (2012).

[13] A. G. Aronov, Y. B. Lyanda-Geller, and G. E. Pikus, Sov. Phys. JETP **73**, 537 (1991).

[14] H. A. Engel, E. I. Rashba, and B. I. Halperin, Phys. Rev. Lett. **98**, 036602 (2007).

[15] L. Meier, G. Salis, I. Shorubalko, E. Gini, S. Schön, and K. Ensslin, Nat. Phys. **3**, 650 (2007).

[16] B. A. Bernevig and S. C. Zhang, Phys. Rev. B **72**, 115204 (2005).

[17] B. M. Norman, C. J. Trowbridge, J. Stephens, A. C. Gossard, D. D. Awschalom, and V. Sih, Phys. Rev. B **82**, 081304(R) (2010).

[18] G. Dresselhaus, Phys. Rev. **100**, 580 (1955).

[19] Y. A. Bychkov and E. I. Rashba, J. Phys. C **17**, 6039 (1984).

[20] G. E. Pikus and A. N. Titkov, in *Optical Orientation*, edited by F. Meier and B. P. Zakharchenya (Elsevier Science, Amsterdam, 1984).

[21] J. J. Baumberg, S. A. Crooker, D. D. Awschalom, N. Samarth, H. Luo, and J. K. Furdyna, Phys. Rev. B **50**, 7689 (1994).

[22] See Supplemental Material at http://link.aps.org/supplemental/10.1103/PhysRevLett.112.056601 for a discussion of anisotropic spin relaxation and the steady-state spin polarization.

[23] Y. Qi, Z. G. Yu, and M. E. Flatté, Phys. Rev. Lett. **96**, 026602 (2006).